JOURNAL OF MATERIALS SCIENCE 25 (1990) 391–398

The influence of Cu and Mg additions on the decomposition of Al–(40 to 50) wt% Zn alloys during isothermal and continuous heating

A.-M. ZAHRA, C. Y. ZAHRA
Centre de Thermodynamique et de Microcalorimétrie du CNRS, 26 rue du 141e R.I.A., 13003 Marseille, France

J. DUTKIEWICZ, R. CIACH
Institute for Metal Research, Polish Academy of Sciences, 30059 Krakow, ul. Reymonta 25, Poland

The influence of 1 wt% copper and 0.2 wt% magnesium additions on the heat evolution and structural changes of Al–40 and Al–50 wt% Zn alloys during isothermal ageing at 30° C and continuous heating up to 400° C was studied using microcalorimetry, differential scanning calorimetry and transmission electron microscopy. Isothermal studies indicate rapid formation of Guinier–Preston (GP) zones at initial stages of ageing followed by discontinuous precipitation of β-phase competing with the formation of transition phases also containing third elements. DSC curves show that the amount of metastable phases formed during room temperature ageing increases with ternary additions, especially to Al–50% Zn alloys. Up to 75° C, GP zones undergo composition but no size changes: during further continuous heating, η' (Mg_2Zn) appears, the dissolution of which proceeds parallel to the continuous precipitation of β at medium temperatures. Addition of copper reduces the discontinuous β-precipitation to a lesser extent than magnesium.

1. Introduction

In zinc-rich aluminium alloys, the high-temperature solid solution, α', decomposes either according to a discontinuous reaction yielding the equilibrium phases α (solute-depleted matrix) and β (nearly pure zinc) or via periodically grown Guinier–Preston (GP) zones and other metastable states (α'_r, α'_m, β_m). The discontinuous precipitation leads to a lamellar structure showing poor mechanical properties; however, it is a major mechanism of decomposition for alloys exceeding 30 wt % Zn [1–3].

It is already known that small additions of third elements, such as copper, iron, silicon and magnesium, reduce the extent of discontinuous precipitation in Al–Zn alloys [4–11]. Results from the studies of Ciach *et al.* [6], Löffler *et al.* [7] and Simerska *et al.* [8] show that magnesium significantly retards the discontinuous precipitation and the overall rate of zinc precipitation. It also has a decreasing effect on the size of the Guinier radius for GP zones and of the transition α'_r-phase compared to binary Al–Zn alloys. The addition of 0.5 to 3% Cu also diminishes the wavelength of zinc-rich fluctuations [10, 11] and slows down the zinc precipitation similar to magnesium.

Thus, third elements slow down the growth process of colonies of discontinuous precipitates by localizing themselves at the interfaces of the lamellae, thus reducing their mobilities, or by trapping vacancies. They also modify the position of GP zone and β-phase solvi in the Al–Zn system [1, 4, 5] and cause the precipitation of other phases, i.e. η and η' in the presence of magnesium [6–8] and ε and T in the presence of copper [9, 12].

In the present study, thermal measurements were used for the first time to study these effects in Al–(40 to 50) wt % Zn alloys. Small additions of magnesium and copper were chosen in order to investigate their effects on the mechanism of β-phase formation without significant interference of other ternary phases. The calorimetric measurements were completed by electron microscopic observations of isothermally aged and continuously heated alloys.

2. Experimental procedure

Alloys were cast starting from 99.99% pure elements. They correspond to the compositions (wt %) given in Table I, determined by atomic emission spectrometry.

Specimens 1 mm thick were annealed at 360° C for 2 d in order to eliminate the dendritic segregation.

TABLE I

Alloy	Zn	Cu	Mg	Al
A	40.1	–	–	balance
B	39.6	–	0.20	balance
C	39.6	0.96	–	balance
D	49.6	–	–	balance
E	49.1	–	0.22	balance
F	49.4	0.70	–	balance

0022–2461/90 $03.00 + .12

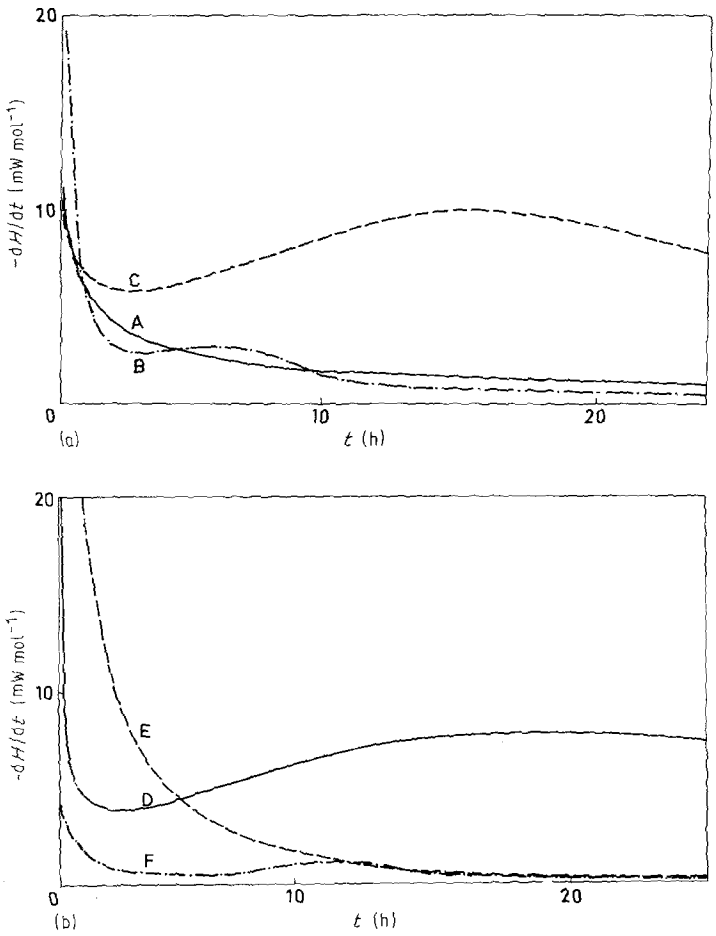

Figure 1 Heat flows accompanying the ageing at 30° C of solid solutions water-quenched from 400° C. (a) A, Al–40% Zn; B, Al–40% Zn–0.2% Mg; C, Al–40% Zn–1% Cu. (b) D, Al–50% Zn; E, Al–50% Zn–0.2% Mg; F, Al–50% Zn–1% Cu.

They were then homogenized for 2 h at 400° C before being quenched into iced water.

Isothermal studies of the heat flow dH/dt were performed with the help of a Tian–Calvet microcalorimeter kept at 30° C. Twenty samples having a diameter of 15 mm were introduced into the thermoelectric pile after the quenching operation. The resulting perturbation of the thermal equilibrium of the apparatus did not allow reproducible measurements before 30 min; the experiments were carried out over several days.

For each differential scanning calorimetry (DSC)-run, one disc, 6 mm diameter, was used in the aged state; after water quenching, the samples were kept at room temperature (RT) for 30 min or 7 d. A Dupont thermal analyser, model 990, was employed at two heating rates (5 and 20° C min^{-1}) between −5 and 400° C. The experimental curves are represented in such a way as to permit direct comparison of the different peak areas, and hence of enthalpy changes observed during heating.

For the structural studies, the aged alloys were mechanically ground down to about 0.1 mm and electrolytically thinned at −30° C in a solution consisting of 25% HNO_3 and 75% CH_3OH, using a Tenupol Struers jet electropolishing apparatus. A transmission electron microscope, Philips type EM 400, was employed at 120 kV.

3. Results and discussion

3.1. Isothermal microcalorimetry

The heat flows which accompany the decomposition of water-quenched solid solutions containing 40% and 50% Zn as well as magnesium or copper additions are shown in Figs 1a and b; the ageing temperature is 30° C. Each curve starts with a powerful heat output which falls off rapidly except for curve E. Curves C and D show a second maximum; the latter is smaller in curves B and F and absent in curves A and E. The heat evolution becomes negligible after 50 h ageing in alloys A, B, E and F but, it is still high in alloys C and D.

The initially very important heat effects characterize the rapid disintegration of the supersaturated solid solution; metastable phases appear most probably according to the spinodal decomposition mechanism [1, 12, 13]. The overlapping effects which start early and pass by a maximum are indicative of a nucleation and growth process; they accompany the formation of either a metastable phase which encounters diffusion problems (due to a low vacancy supersaturation, for example) or of the β-phase according to the discontinuous precipitation reaction [14]. The latter mechanism leads to a predominantly lamellar or globular morphology as observed previously [12, 13] for Al–(50 to 60)% Zn.

3.2. DSC studies

DSC experiments permit the detection indirectly of which phases are present in aged alloys and how they evolve during continuous heating. This is exemplified on solid solutions aged at RT for 7 d: Fig. 2 shows curves for the Al–40% Zn alloy series examined at 5° C min^{-1}, Fig. 3 those for the Al–50% Zn alloy series at 20° C min^{-1}. Several endo- and exothermal heat effects overlap so that their interpretation becomes

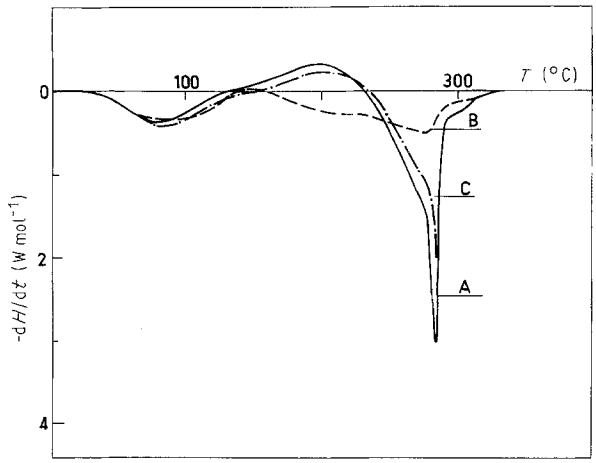

Figure 2 DSC curves of alloys A, B and C quenched from 400° C, aged 7 d at RT, then heated at 5° C min^{-1}.

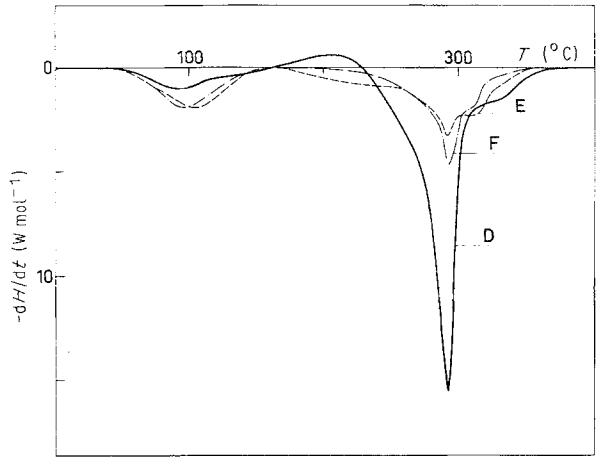

Figure 3 DSC curves of alloys D, E and F quenched from 400° C, aged 7 d at RT, then heated at 20° C min^{-1}.

difficult. A comparison of these curves shows that the first endotherm decreases with rising zinc concentration and increases when ternary elements are added; it corresponds to the dissolution of metastable phases. They transform partially into more stable ones upon slow heating; in fact, the endothermal effects measured at 5° C min^{-1} are in general smaller than those measured at 20° C min^{-1}.

In Fig. 2, alloy B starts with a double reversion peak still visible at 20° C min^{-1}. Important net exothermal effects appear in alloys A and C during further heating; their temperature level corresponds to α'- and β-precipitation which is suppressed at higher rate.

Exothermal effects are also observed upon slow heating of alloys D, E and F; at the higher rate, they appear only for alloy D (Fig. 3).

In the course of further heating, some β is dissolved, as the zinc solubility increases strongly with a rise in temperature. The corresponding endothermal effect merges above 270° C into one which accompanies the monotectoid reaction: $\alpha + \beta \rightarrow \alpha + \alpha'$. The magnitude of the latter increases with increasing zinc concentration and decreases in the presence of ternary elements; a small addition of magnesium is especially effective in reducing its amount.

At still higher temperatures, the single-phase region is attained after the crossing of the two-phase field ($\alpha + \alpha'$). If the solid solution has only been aged for 30 min at RT, the precipitation of metastable and stable phases upon heating provokes strong exothermal effects.

3.3. Transmission electron microscope observations

In order to follow structure changes during continuous heating, transmission electron microscopy was used after heating at 5° C min^{-1} to certain temperatures corresponding to characteristic heat effects. Fig. 4 shows micrographs of alloys A, B and C heated to 75° C, all taken at $\boldsymbol{g}$ = [1 1 1] operating in order to show modulations in the [1 1 1] direction. It can be seen that alloy A does not exhibit a very pronounced directional dependence, while in alloys with additions, modulations are clearly perpendicular to the [1 1 1] direction, i.e. follow (1 1 1) planes. This indicates earlier transformation of periodical spherical GP zones into ellipsoidal ones. At 1 1 1 reflections, clear side-band reflections can be seen. From measurements of the average distance of GP zones or calculations of the wavelength from the distance of side bands marked in the electron diffraction patterns according to a formula used in a previous paper [15], the wavelength for these alloys is found to be in the range 0.3 to 0.4 nm which is in agreement with measurements from the micrographs. This result is close to that measured in alloys aged 7 d at RT and indicates that

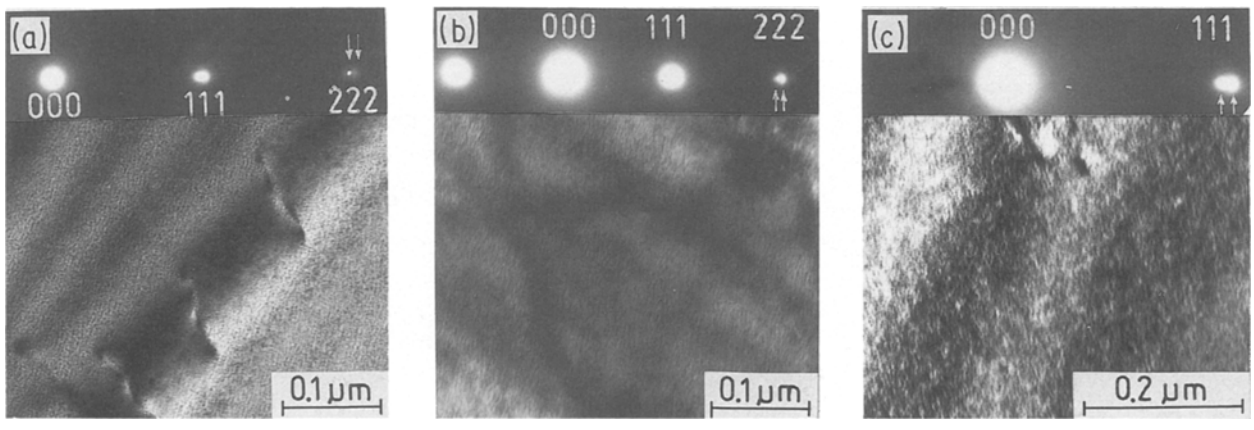

Figure 4 Transmission electron micrographs of alloys (a) A, (b) B and (c) C aged 7 d at RT and heated to 75° C at 5° C min^{-1}. Upper part: 1 1 1 row of reflections of corresponding selected-area diffraction pattern (SADP).

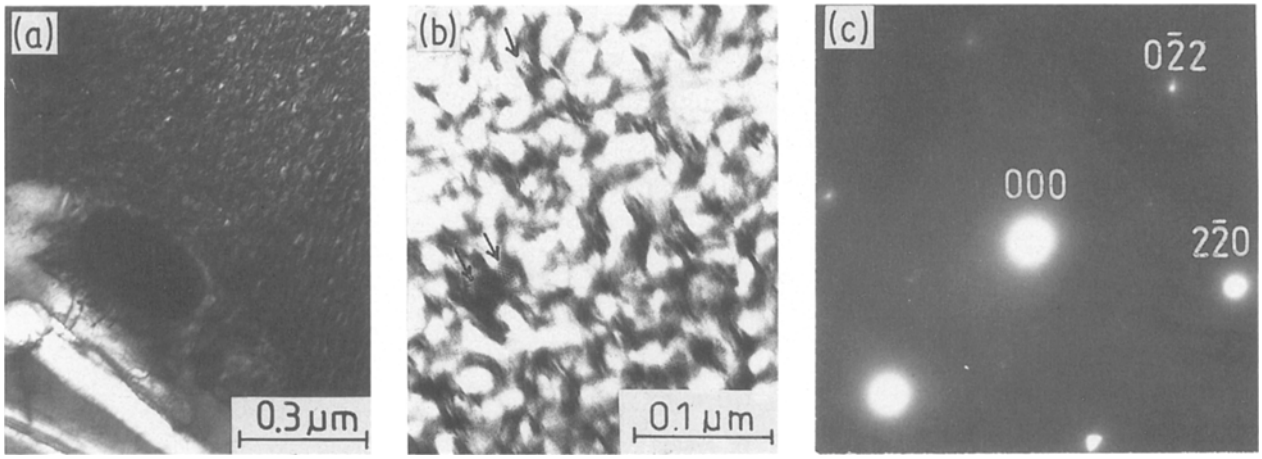

Figure 5 Alloy A heated to 200° C at 5° C min^{-1}: (a) region of a grain boundary, (b) continuous precipitates at [1 1 1] zone axis orientation, (c) corresponding SADP.

during heating to 75° C, GP zones do not grow at the expense of smaller ones, but rather change composition. Okuda *et al.* [16] have observed decreasing solute concentrations during the early stage of reversion, supporting this observation. The presence of side bands indicates well-developed periodicity of GP zones, which may have its origin in the spinodal decomposition mechanism.

Alloys A and C were also examined after heating to 200° C where maximum heat evolution occurs. Their behaviour was similar. Microstructures of alloy A are given in Figs 5a to c. Fig. 5a shows discontinuous precipitates at a grain boundary, and continuous precipitates that can be seen better in (b) at [1 1 1] zone axis orientation. The thickness of the plates is at this stage more than 10 nm, exceeding the critical size of 6 nm [17] which allows the formation of α_r'-transition phase by inserting an extra $\{1\,1\,1\}$ plane. From the electron diffraction pattern (c), weak $0\,1\,\bar{1}\,0$ reflections and splitting of basic reflections are seen to occur due to the presence of the α_r'-phase, visible better at other orientations. In a few places, Moiré patterns can be seen (marked by arrows in Fig. 5b) as already observed by Ramlau and Löffler [17] at this orientation due to β-formation within α_r'.

Owing to the different character of the DSC curve for alloy B (Fig. 2), its structure was studied after heating to 145 and 210° C. Fig. 6 shows micrographs

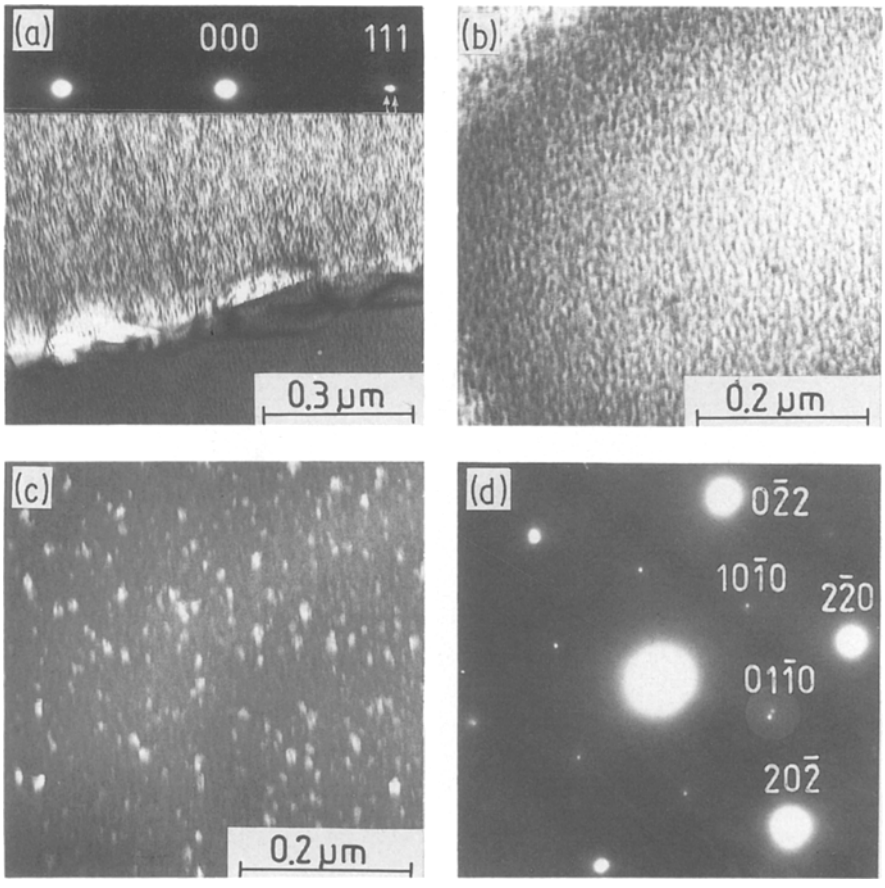

Figure 6 Alloy B heated to 145° C at 5° C min^{-1}: (a) region of a grain boundary with 1 1 1 row of reflections from SADP in the upper part, (b) microstructure taken at [1 1 1] zone axis orientation, (c) dark-field (DF) micrograph taken using $0\,1\,\bar{1}\,0$ β-reflection, (d) corresponding SADP.

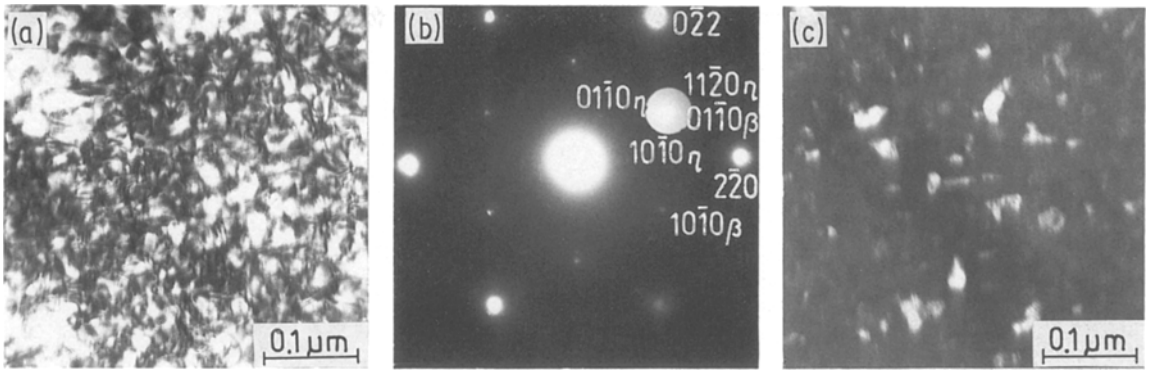

Figure 7 Alloy B heated to 210° C at 5° C min^{-1}: (a) microstructure taken at [1 1 1] zone axis orientation, (b) corresponding SADP, (c) DF microstructure taken using 0 1 $\bar{1}$ 0 β-reflection.

relative to 145° C. In Fig. 6a only single β-precipitates at the grain boundary can be seen together with a coarse modulated structure perpendicular to {1 1 1} planes. Side-band reflections are closer to the fundamental spots and the wavelength calculated from their spacing is within the range 7 to 8 nm. Fig. 6b shows a modulated structure at [1 1 1] zone axis orientation. β reflections, indicating [0 0 0 1] zone axis orientation, are present in the diffraction pattern (d). The dark-field micrograph (c) taken with the 0 1 $\bar{1}$ 0 β spot shows a high density of continuously formed β-precipitates of sizes 5 to 20 nm.

The next set of micrographs (Fig. 7) taken of alloys at identical [1 1 1] zone axis orientations shows interesting features after heating to 210° C. The bright-field micrograph (a) indicates large precipitates with Moiré pattern in ⟨1 1 1⟩ and ⟨2 1 1⟩ directions. As can be seen from the indexing of the diffraction pattern (b), it contains η' and β-precipitates at (0 0 0 1) orientation. The dark-field micrograph (c) taken using 0 1 $\bar{1}$ 0 β and 1 1 $\bar{2}$ 0 η' spots shows various sizes of precipitates and also Moiré patterns resulting from differences in lattice spacings of $d_{11\bar{2}0\,\eta'}$ and $d_{01\bar{1}0\,\beta}$ of overlapping precipitates. Hence the structure may explain the different evolution of the DSC curve for alloy B. Whereas the low-temperature behaviour is similar in all three alloys, at least two heat effects overlap in alloy B at medium temperatures. They may be attributed to the appearance of continuously formed β which is more pronounced in the presence of magnesium (cf. Figs 5 and 7), and to the dissolution of the η'-phase which has been formed upon heating from magnesium-containing GP zones [18].

Fig. 8 shows a transmission electron micrograph of alloy D after quenching and ageing for 7 d at RT. Some part of the volume has already decomposed by a discontinuous mode, while modulations can also be seen. The electron diffraction pattern (b) shows side bands near 1 1 1 and 2 2 2 reflections. From the distance of side bands and direct measurements from the micrograph, the wavelength of the composition modulations was estimated to be about 4 nm.

Micrographs of alloys D, E and F heated to 75° C were taken at $\boldsymbol{g}$ = [1 1 1] orientation (Fig. 9). The modulated structure seems to be coarser than in the Al–40% Zn alloy series, but measurements of the side-band distance does not confirm this observation. Microstructures show dark spots (marked by arrows) which grow during observation and were identified as *in situ* nucleated β-precipitates. This may indicate that the modulated structure is affected by *in situ* growth effects. The modulations' wavelength calculated from the side-band distance at 1 1 1 and 2 2 2 reflections (Figs 9a and b) is equal to about 4 nm, close to that calculated for alloy D aged 7 d at RT (Fig. 8).

During further continuous heating of alloy D to 210° C, the mean distance between metastable precipitates increases to about 20 nm, as can be seen from Fig. 10. The growth of continuous precipitates retards the progress of discontinuous precipitation. At this

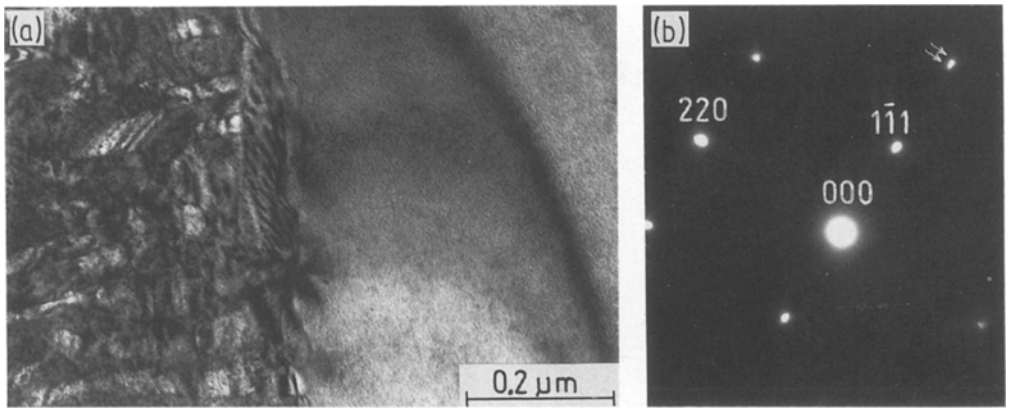

Figure 8 Alloy D aged 7 d at RT: (a) microstructure of a grain-boundary region, (b) SADP from the area of continuous precipitates.

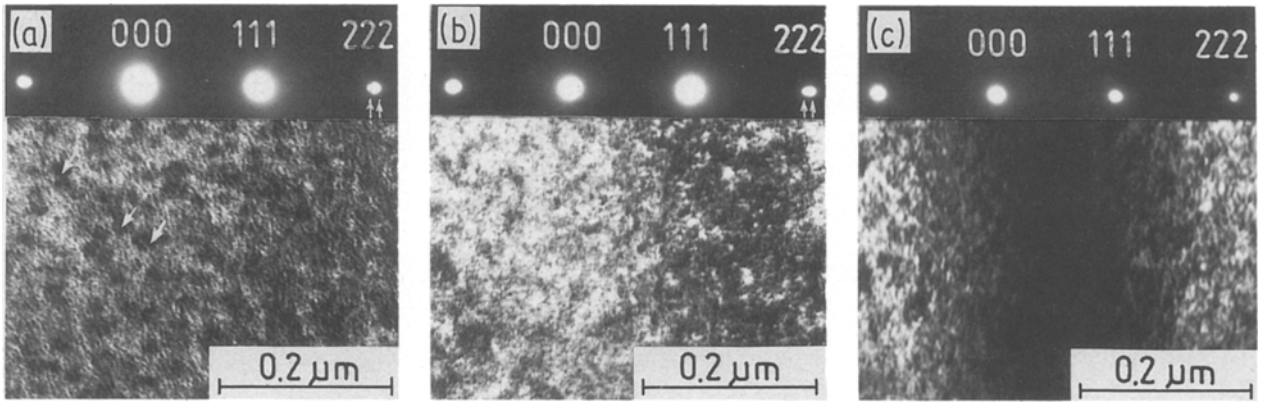

Figure 9 Micrographs taken from alloys (a) D, (b) E and (c) F heated to 75° C at 5° C min^{-1}. 1 1 1 rows of reflections of corresponding SADP are shown in the upper parts of figures.

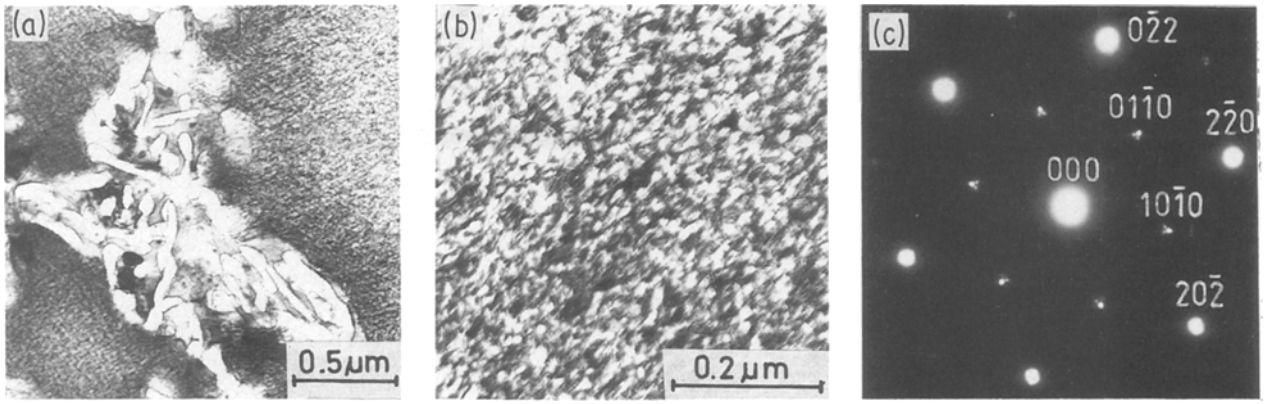

Figure 10 Alloy D heated to 210° C at 5° C min^{-1}: (a) microstructure showing discontinuous and continuous precipitation, (b) microstructure taken at [1 1 1] zone axis orientation, (c) corresponding SADP.

stage of ageing a transition α_r'-phase is formed within the zinc-rich modulations causing significant splitting of reflections in $\langle 1\,1\,0 \rangle$ directions and medium intensity 0 1 $\bar{1}$ 0 type β-reflections appear at [1 1 1] zone axis orientation (c). The splitting of 0 1 $\bar{1}$ 0 reflections may indicate formation of the β_m transition hexagonal phase of larger lattice constants as suggested by Ramlau and Löffler [17]. It shows a slight tilt with respect to the ideal orientation relationship due to a rotation of (1 1 1) planes within the α_r'-phase. The splitting of 0 1 1 0 β-reflections may, however, also be caused by double diffraction due to the existence of the α_r'-phase with a small lattice mismatch to the α-phase.

Fig. 11 shows a transmission electron microstructure taken at [1 1 1] zone axis orientation after heating alloy E to 135° C. As can be seen from the electron diffraction pattern (b), β-reflections of significant intensity exist, similar to those in Fig. 10c. In a few places in (a), a Moiré pattern appears due to interference of 0 1 $\bar{1}$ 0 of β with β_m-reflections. No η-reflections can be seen at this stage of ageing.

Fig. 12 represents microstructures of the same alloy taken at [0 0 1] zone axis orientation. It shows precipitations elongated in the $\langle 1\,1\,0 \rangle$ direction. As can be seen from the electron diffraction pattern (c), the fundamental reflections do not show splitting in $\langle 1\,1\,0 \rangle$ directions as in Fig. 10c, but new weak

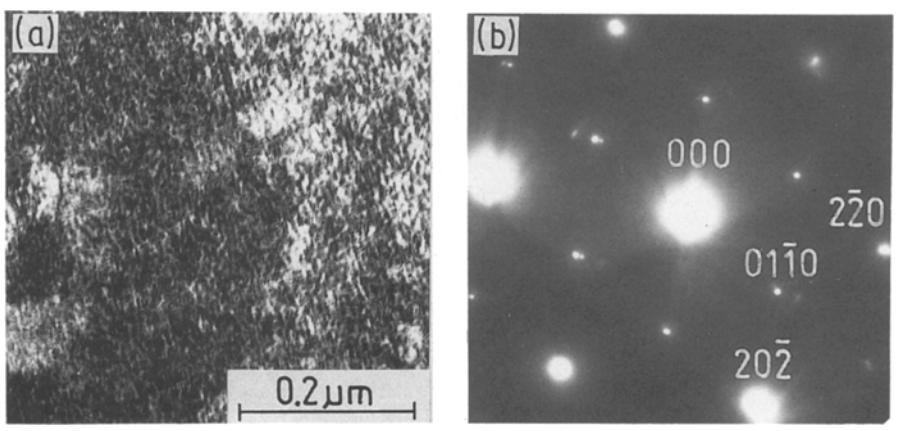

Figure 11 Alloy E heated to 135° C at 5° C min^{-1}: (a) microstructure taken at [1 1 1] zone axis orientation, (b) corresponding SADP.

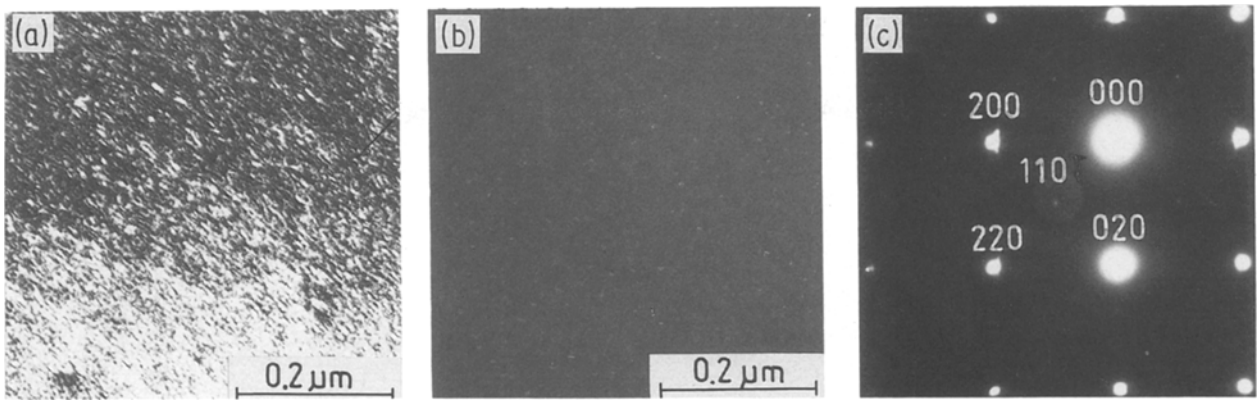

Figure 12 Alloy E heated to 135° C at 5° C min^{-1}: (a) microstructure taken at [0 0 1] zone axis orientation, (b) DF micrograph taken using reflection placed in superlattice $(1\,1\,0)_\alpha$ position, (c) corresponding SADP.

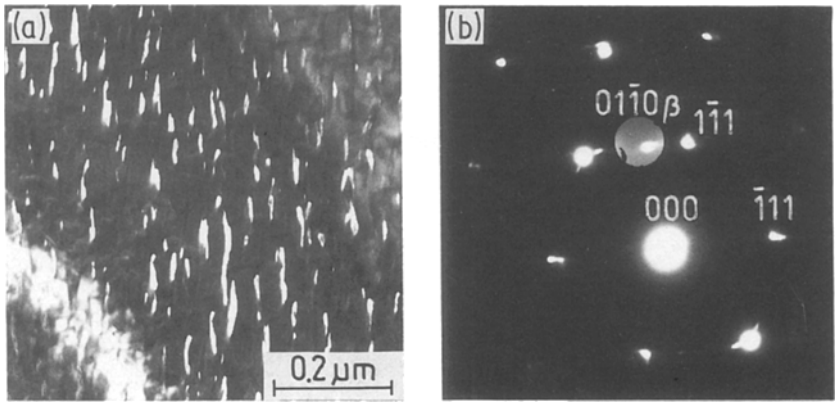

Figure 13 Alloy F heated to 210° C at 5° C min^{-1}: (a) DF micrograph taken using $0\,1\,\bar{1}\,0$ β-reflection, (b) corresponding SADP.

reflections appear in positions corresponding to 1 1 0 α-superlattice reflections. The corresponding dark-field micrograph (Fig. 12b) shows small bright areas in a few cases elongated in $\langle 1\,1\,0\rangle$ directions. They represent either an ordered transition α_r'-phase or correspond to the 0 0 0 2 η'-reflection according to the relationship $(0\,0\,0\,1)\,\eta' \parallel (1\,1\,0)\,\alpha$ as stated by Löffler *et al.* [19].

The last micrograph (Fig. 13) represents the structure of alloy F heated to 210° C; it was taken using $0\,1\,\bar{1}\,0$ β-reflection at [1 1 0] α-zone axis orientation and shows elongated β-precipitates of various sizes. It indicates the advanced stage of β-formation from the continuous α_r'-precipitates. The electron diffraction pattern (b) also shows a splitting of reflections in $\langle 1\,1\,1\rangle$ directions, much larger than it arises from the α_r'-phase, which is most probably caused by the presence of a copper-containing phase.

4. Conclusions

1. Isothermal microcalorimetric and transmission electron microscopic studies show that at 30° C, mainly metastable phases appear in Al–40% Zn alloys; at still higher zinc contents, the discontinuous precipitation of the equilibrium phase competes with the continuous precipitation mechanism; the former becomes rapidly preponderant.

2. DSC measurements indicate that the amount of metastable phases formed during RT ageing increases in the case of small magnesium and copper additions, especially to the Al–50% Zn alloy. These phases transform partially into more stable ones, to an increasing extent with decreasing heating rates. The first endothermal peak is connected with a solute concentration change within GP zones, because no significant change in the distance of the composition modulations is observed. Exothermal effects in binary alloys are mainly due to α_r'- and β-precipitation within modulations of much larger distance.

3. The addition of 0.2% Mg to Al–(40 to 50)% Zn alloys has no significant effect on the wavelength of the modulations in the primary ageing state. It causes, however, the formation of magnesium- and zinc-containing GP zones which transform during further heating into η'-phase. The β-precipitation by the continuous mechanism begins earlier and proceeds to a higher extent than in the binary alloys.

4. Magnesium and copper additions limit the extent of discontinuous β-precipitation, magnesium being the more efficient. This inhibition may be due to the trapping of vacancies and/or to the formation of η'-precipitates (in magnesium-containing alloys) or a copper-rich transition phase (in copper-containing alloys) hindering the discontinuous precipitation front.

References

1. H. LÖFFLER, V. SYNECEK, M. SIMERSKA, G. WENDROCK, P. BARTUSKA and R. KROGGEL, *Phys. Status Solidi* (*a*) **65** (1981) 197.
2. M. SIMERSKA, P. BARTUSKA and V. SYNECEK, *Acta Crystallogr.* **A34** (1978) Part S4, 304.

4. P. BARTUSKA, M. SIMERSKA and V. SIMA, *Czech. J. Phys.* **B25** (1975) 1139.
5. M. SIMERSKA and P. BARTUSKA, Proceedings of the 6th European Crystallography Meeting, Barcelona, p. 213.
6. R. CIACH, J. DUTKIEWICZ, J. SALAWA and W. BALIGA, *Arch. Hutn.* **19** (1974) 149.
7. H. LÖFFLER, G. WENDROCK, B. MAJOR, J. DUTKIEWICZ, J. KROL and M. HAMANKIEWICZ, *ibid.* **30** (1985) 531.
8. M. SIMERSKA, B. MAJOR, V. SYNECEK, P. BARTUSKA and W. BALIGA, *Arch. Metall.* **32** (1987) 421.
9. J. KROL, B. MAJOR, K. SACKEWITZ and G. WENDROCK, *Wiss. Z. Paed. Hoch. "N.K. Krupskaja", Halle* **15** (1977) 30.
10. R. CIACH, J. DUTKIEWICZ, H. LÖFFLER and G. WENDROCK, Proceedings of the Conference on Applied Crystallography, Kozubnik (1978).
11. R. CIACH, H. LÖFFLER, J. SALAWA and G. WENDROCK, *Phys. Status Solidi (a)* **53** (1979) 441.
12. J. DUTKIEWICZ, *Prace Komisji Met.-Odl. PAN, Krakow* **18** (1974) 53.
13. R. CIACH, J. DUTKIEWICZ, R. KROGGEL, H. LÖFFLER and G. WENDROCK, *Krist. Techn.* **10** (1975) 123.
14. A. ZAHRA, C. Y. ZAHRA and R. CIACH, *J. Therm. Anal.* **26** (1983) 303.
15. R. KROGGEL and J. DUTKIEWICZ, *Cryst. Res. Technol.* **18** (1983) 1555.
16. H. OKUDA, K. OSAMURA, H. HASHIZUME and Y. AMEMIYA, *Acta Metall.* **36** (1988) 899.
17. R. RAMLAU and H. LÖFFLER, *Godis Jugoslav. Centra za Kristalog.* **20** (1985) 31.
18. A. ZAHRA, C. Y. ZAHRA, M. LAFFITTE, W. LACOM and H. DEGISCHER, *Z. Metallkde.* **70** (1979) 172.
19. H. LÖFFLER, I. KOVACS and J. LENDVAI, *J. Mater. Sci.* **18** (1983) 2215.

Received 3 October 1988
and accepted 28 February 1989